SI APPENDIX- Negron-Oyarzo et al. 2018

1. SI Material and Methods

Animals. C57BL/6j mice (n = 10) were used in this study. Mice were housed in a temperature and humidity controlled room (22 ± 2°C) with food and water *ad libitum*. All experimental procedures related with animal experimentation were approved by Institutional Animal Ethics Committee of the Pontificia Universidad Catolica de Chile (protocol code: CEBA-12-040). Efforts were made to minimize the number of animals used and their suffering.

Microdrive. Custom-made microdrives carrying four tetrodes were assembled for simultaneous electrophysiological recording of local field potential (LFP) in the prefrontal cortex and the dorsal CA1 area of the hippocampus and single-units in the prefrontal cortex. Tetrodes were constructed from four twisted 17 um polyimide-coated nichrome wires (A-M Systems; WA, USA). Final impedance of each wire was adjusted to ~1 MOhm measured in gold solution at 1 kHz with an impedance tester (model Omega-tip-Z, WPI; MA, USA). Microdrives were composed of two bundles of four stainless-steel cannula each (30 G; Components Supply Co, FL, USA). Three tetrodes were inserted in the bundle targeting the prefrontal cortex, and one tetrode in the bundle targeting the hippocampus. Each tetrode was cemented to a single movable shuttle fixed with a screw to allow independent regulation of depth (full twist: ~300 µm). Tetrodes were connected to a 16 channels-printed circuit board assembled to an Omnetics connector.

Surgery. Animals of 60 days of age were used for implantation of microdrives. Animals were initially anesthetized with isoflurane (4% isoflurane with 100% O_2) before being placed in a stereotaxic frame, and anesthesia was maintained using isoflurane (1–2% isoflurane with 100% O_2) until the surgery was finished. Rectal temperature was monitored, and core temperature (37°C) was maintained with a heating pad (Harvard Apparatus, MA, USA). After incision in the scalp, two burr holes were drilled in the right hemisphere at stereotaxic coordinates targeting prefrontal cortex (1.94 mm AP, 0.5 mm ML, from Bregma) and region CA1 of the hippocampus (-1.54 mm anterior, 1.5 mm lateral from Bregma). The dura was removed, and the electrodes were lowered to the cortical surface. Two ground wires were attached to skull screws, and the microdrive was affixed to the skull with dental acrylic. All electrodes were immediately lowered two full turns (~600 µm) into the cortex. After surgery, animals were maintained in individual cages in a room with temperature (22 ± 2°C) and humidity controlled with food and water *ad libitum.* Mice were allowed to recover for one week after surgery before beginning behavioral experiments. During recovery, weight and general health was monitored daily, and animals received an intraperitoneal dose of

www.pnas.org/cgi/doi/10.1073/pnas.1720117115

analgesic (Ketoprofen, 5 mg/kg/day) and antibiotic (Enrofloxacine, 5 mg/kg/day). Microdrives allowed stable recording for up to two months.

Recordings. After a week of recovery from surgery, mice were placed in a custom-built booth, and microdrives were connected to a headstage (model RHD2132 Intan Tech, CA, USA). Neural signals were amplified (200 times), digitized (sampled at 20 kHz) filtered 0.5–5000 Hz, and monitored through amplifier board (RHD2000 evaluation system; Intan Tech, CA, USA). Tetrodes were lowered individually to the target regions by ~0.5 mm/day, in ~0.15 mm increments over several days until detection of single units in the prefrontal cortex (~1000-2500 µm of depth) and detection of sharp-wave ripples in the CA1 of hippocampus (~1500 µm of depth) was evident. Once tetrodes had reached their desired locations, behavioral experiments started.

Behavioral experiments. Mice were trained for spatial reference memory in the Barnes maze (1). The maze consisted of a white circular platform of 70 cm diameter elevated at 70 cm from the floor with 16 equally spaced holes along the perimeter (9 cm diameter each) located at 2 cm from the edge of the platform. Visual cues were located on the walls of the room. Under one of the holes was located a black plexiglass escape-box (17 × 13 × 7 cm) that allows the entrance of the mice with the microdrive implanted. The location of the escape-box was consistent for a given mouse, but randomized across mice. The maze was rotated daily, with the spatial location of the target unchanged with respect to the distal visual room cues to prevent a bias based on olfactory or the proximal cues within the maze. The maze was illuminated with two incandescent lights to yield a light level of ∼400 lux impinging on the circular platform.

For habituation, mice were placed in the start-box (18 x 15 x 10 cm) in the center of the maze for 1 min, then the start box was lifted, and the animal was guided to the escape-box with the room lights turned off. After 1 min, the mouse was removed from the escape-box and returned to the start-box for three additional training sessions into the escape-box. During habituation, mice were not connected to the amplifier recording system. In each navigation trial, mice were placed in the start-box for 1 min with the room lights turned off (start phase). After time had elapsed, the start-box was removed and the mouse was free to explore the maze (navigation phase). The session ended when the mouse entered the escape-box or after 3 min elapsed. When the mouse entered the escape-box, the lights were turned off and the mouse was allowed to remain in the escape-box for 1 min (goal phase). If the mouse did not find the escape-box within 3 min, the experimenter guided the mouse to the escape. Once the trial was completed, the mouse was disconnected from the electrophysiological recording system, and was returned to the home cage. For every mouse, four navigation trials per day with an inter-trial interval of 15 min during 4 consecutive days were applied. To evaluate the recall of reference spatial memory a probe

trial without the escape-box of 90 s was conducted 24 h after the last acquisition trial. Animal behavior was tracked and recorded with a web-cam (acquisition at 30 fps and 640 x 480 pixels; camera model C920; Logitech Co.) located 1 mt above the maze and controlled with VirtualDub software. Videos were stored in a hard-disk for off-line analysis.

Histology. After completion of experiments, mice were anesthetized with 1 % isofluorane, and the location of each tetrode was marked by passing a small amount of current through each tetrode (50 μA for 10 s). At the next day, mice were anesthetized with isofluorane (3%), and then transcardially perfused with 20 ml of saline solution followed by 50 ml of 4% paraformaldehyde in phosphate buffer saline (PBS, pH = 7.4). The brain was removed, incubated overnight in 4% paraformaldehyde in PBS and then stored in PBS containing 0.2% sodium azide. Coronal brain slices (60 μm) were prepared from paraformaldehyde-fixed brains with vibratome (World Precision Instruments, Sarasota, USA) in ice-cold PBS. For visualization of the electrolytic lesions, slices were stained with Nissl-staining, and images were acquired with microscope (Nikon).

Data Analysis.

Animal behavior. Behavioral performance was analyzed measuring the latency time to enter the escape-hole and number of errors, defined as nose-pokes in non-escape holes (2). In probe trials, we measured the percentage of trial time that the animal spent in the target quadrant during the first 30 seconds of the trial session. To assess locomotor activity we measured mean and maximum speed in all trials. All these behavioral parameters were measured with ANY-maze software (Stoelting Co.). Navigation strategies were classified as previously described (3), with slight modifications. For evaluation of navigation strategies, the maze was divided into four equal quadrants, in which the escape-hole was in the center of the target quadrant. Strategies were classified as spatial, in which mice moved directly to the target quadrant, and sometimes directly into the escape-hole; or non-spatial, which included movement to non-target quadrants, failures to solve the task, or apparently random or serial nose-pokes into error holes.

Locomotor patterns. IdTracker, an open source video tracking system (4), was used to automatically collect the mouse's instantaneous position along the track. The animal trajectory was smoothed (mobile mean of 10 successive points) to avoid artifacts due to space discretization and the animal's instantaneous speed was quantified as the mean displacement between adjacent frames divided by the frame time (camera acquisition at 30 fps). A period of navigation was operationally defined as an interval of movement with instantaneous speed above 0.1 cm/s and lasting at least 2 s. Other parameter values yielded qualitatively similar results.

LFP spectral power and coherence. For analysis of power of oscillatory activity, electrophysiological recording were downsampled to 1000 Hz, bandpass-filtered at 0.1–100

Hz, and power spectral density (PSD) and coherence were computed using multitaper Fourier analysis (5) from the Chronux toolbox (http://www.chronux.org). For PSD analysis, field potentials were divided into 5000 ms segments with 500 ms overlap, and a time-bandwidth product (TW) of 3 and 5 tapers. For spectral coherence, field potentials were divided into 2000 ms segments with 100 ms overlap, and a time-bandwidth product (TW) of 5 and 9 tapers. Mean spectral power and coherence measures were calculated for theta (6–10 Hz), slow-gamma (20–40 Hz), and fast-gamma (60–80 Hz) bands for the entire trial session, and separately for start, navigation and escape phases of the task.

Spike sorting. Spike sorting was performed offline using MATLAB based graphical cluster-cutting software, Mclust/Klustakwik-toolbox (version 3.5; (6)). To detect spikes, broadband recordings sampled at 20 kHz were filtered at 600-5000 Hz, and events with amplitudes reaching 5-50 standard deviations over the mean were considered as candidate spikes. For each recording file, single channels from individual tetrodes were identified, and a single file was generated per channel. Then all four generated files from the same tetrode were clustered by Principal Components Analysis (PCA) using MClust 3.5 toolbox running on MATLAB. The spike features considered for clustering included peak amplitude (the maximum height of the waveform of each channel of each spike), timestamp (the time of occurrence of each spike), spike width (the duration in each channel of each spike), energy (the energy contained within the waveform of each channel of the spike), valley (the maximum depth of the waveform of each channel of the spike), and wave-PC (the contribution to the waveform due to the principal component). This analysis generated between 5-20 clusters per tetrode, and for each cluster we displayed the average spike waveform for each unit of each tetrode channel, and the number of total putative spikes and average inter-spike interval (ISI). MClust automatically identified similar clusters by assigning values between 0.0-1.0 for each cluster, in which similar clusters displayed values close to 1.0. Similarity between clusters were manually confirmed though visual inspection of spike features. Thus, clusters from a single tetrode that displayed similar values assigned by MClust, and similar spike features (waveform in the same tetrode channel and firing rate) were re-clustered as the same unit. Final confirmation was done examining the ISI for every single unit and establishing that no spikes were present at ISIs shorter than 2 ms. Finally, a file for every single unit including timestamps of spikes for every tetrode was generated and exported, and this file was used in the subsequent analysis on MATLAB. To confirm the correct sorting of single units, timestamps of every single unit was aligned with its 500 Hz filtered LFP recording and the concordance of timestamps with spikes was visually established.

To distinguish fast spiking units from regular spiking units, timestamps of every single unit were aligned with its 500 Hz high-pass filtered LFP recording, and maximum and minimum peaks were detected for every spike (indicated by its timestamp in the filtered LFP). Next, spike amplitude (absolute voltage difference between the spike minimum and maximum) and spike duration (measured as full width at half maximum amplitude) was calculated for

every spike and averaged for each unit. This analysis also included the firing rate for every unit. These three variables (firing rate, valley duration and spike amplitude) were represented for each unit into a 3D-scatter plot. Given that putative fast spiking units display larger firing rate and longest spike duration as compared with putative regular spiking units (7), k-means clustering algorithm was applied to automatically identify these populations. The analysis showed a hierarchical threshold based on the firing rate; that is, units with firing rate superior than 20 Hz were considered as putative fast spiking units.

Spike-field Coherence. Spike-field coherence was computed using the multitaper Fourier analysis (8) and the Chronux toolbox (http://www. chronux.org). We used 500 data points at 1000 Hz, a time-bandwidth product (TW) of 3 and 5 tapers, resulting in a half width of 0.6 Hz. Significantly modulated units were considered when spike field coherence at theta or slow-gamma frequency bands were superior to 2 standard deviation from mean.

Phase locking. Phase-locking analysis was computed using the Matlab toolbox CircStats (http://philippberens.wordpress.com/code/circstats/). Briefly, LFP traces were bandpass filtered at theta or low-gamma range (4-10 Hz and 20-35 Hz, respectively; zero phase shift non-causal finite impulse filter with 0.5 Hz roll-off). Phase locking was quantified as the circular concentration of the resulting phase distribution, which was defined as mean resultant length (MRL = $(n/Z)^{0.5}$; (9)). The statistical significance of phase-locking was assessed using the Rayleigh test for circular uniformity. To avoid bias we only considered neurons with >50 recorded spikes.

Spatial firing rate maps. Once single units were well separated, auto-scaled color-coded firing rate maps were created to visualize firing rate distributions by dividing the number of spikes with the total time spent by the rat in each pixel. To this aim, spatial position of mice in the maze was obtained from the recorded videos with IdTracker software. The space was divided into 74 x 57 pixel bins (1 bin = 1.58 cm), and firing rate for each bin was calculated and smoothed using Hanning method.

Peri-event time histograms. Activity of prefrontal neurons in turn to events of behavioral relevance was evaluated by cross-correlation applying the “sliding-sweeps” algorithm (10). First, timing of behavioral relevant events, as escape (entering to the escape-hole), nose-poke (nose-poke in the escape hole without entering to the escape box) and errors (nose-poke in non-escape holes) were established by analyzing the recorded videos of behavioral performance using ANY-Maze software. Then, a time window of ±2 s was defined with the 0 point assigned to the start time of the assigned behavioral event. The timestamps of the prefrontal cortex neuronal spikes within the time window were considered as template and represented by a vector of spikes number relatives to t = 0 s, with a time bin of 100 ms and normalized to the total number of spikes. Thus, the central bin of the vector contained the ratio between the number of prefrontal cortex neuronal spikes elicited between ± 100 ms

and the total number of spikes within the template. Next, the window was shifted to successive assigned behavioral events throughout the recording session, and an array of recurrences of templates was obtained. Both prefrontal cortex neuronal spikes timestamps and start times of behavioral events where shuffled by randomized exchange of the original inter-event intervals (11) and the cross-correlation procedure was performed on the pseudo-random sequence. The statistical significance of the observed repetition of spike sequences was assessed by comparing, bin to bin, the original sequence with the shuffled sequence. An original correlation sequence that presented a statistical distribution different from 100 simulated shuffling was considered as statistically significant, with $P < 0.01$ probability, instead of chance occurrence.

Biased firing index. To estimate the selectivity of prefrontal units to fire in turn to entering to the escape-hole during navigation we calculated the index of biased firing to escape for each unit as follows (12):

$$Ib_{(escape)} = \frac{FR_{[escape]}}{FR_{[escape]} + FR_{[error]}}$$

where $Ib_{(escape)}$ is the biased firing index for entering the escape-hole, $FR_{[escape]}$ is the average firing rate 1 s before entering the escape-hole, and $FR_{[error]}$ is the average firing rate 1 s before nose-poke in non-escape holes. To discriminate whether selectivity to discharge was related to entering or finding the escape-hole we also computed the $Ib_{(nose\text{-}poke)}$ as follow:

$$Ib_{(nose\text{-}poke)} = \frac{FR_{[nose\text{-}poke]}}{FR_{[nose\text{-}poke]} + FR_{[error]}}$$

where $Ib_{(nose\text{-}poke)}$ is the biased firing index for nose-poke into the escape-hole but not enter to it, and $FR_{[nose\text{-}poke]}$ is the average firing rate 1 s before entering the escape hole, and $FR_{[error]}$ is the average firing rate 1 s before nose-poke in non-escape holes. $Ib_{(escape)}$ and $Ib_{(nose\text{-}poke)}$ result in values between 0.0 to 1.0, in which 0.0 represents opposite selectivity (i.e.; the unit fires exclusively when the mouse faces an error-hole) and 1.0 is complete selectivity (i.e., the unit fires exclusively when the mouse faces the escape hole).

Statistical analysis. Comparison between behavioral parameters (latency time, errors) and other normally distributed parameters were analyzed with parametric analysis (t-student test; one-way ANOVA followed by Bonferroni post-hoc test). Comparison between firing rates and others non-normally distributed parameters were analyzed with non-parametric tests (Mann-Whitney U-test; Kruskal-Wallis test followed by Dunn's multiple comparison *post-hoc* test). Linear correlations between parameters were analyzed by Spearman correlation test. Comparisons between PETHs were analyzed with Wilcoxon test. Statistical

analysis was performed with Graphpad Prism software or with Matlab (The Mathworks Inc.). Significant differences were accepted at $P < 0.05$. Detailed statistical information for all figures is provided in Table S6.

1. Barnes CA (1979) Memory deficits associated with senescence: a neurophysiological and behavioral study in the rat. *Journal of comparative and physiological psychology* 93(1):74--104.
2. Negron-Oyarzo I, Neira D, Espinosa N, Fuentealba P, & Aboitiz F (2015) Prenatal Stress Produces Persistence of Remote Memory and Disrupts Functional Connectivity in the Hippocampal-Prefrontal Cortex Axis. *Cerebral cortex (New York, N.Y. : 1991)* 25(9):3132--3143.
3. Harrison FE, Reiserer RS, Tomarken AJ, & McDonald MP (2006) Spatial and nonspatial escape strategies in the Barnes maze. *Learning \& Memory* 13(6):809--819.
4. Perez-Escudero A, Vicente-Page J, Hinz RC, Arganda S, & de Polavieja GG (2014) idTracker: tracking individuals in a group by automatic identification of unmarked animals. *Nat Methods* 11(7):743-748.
5. Bowyer SM (2016) Coherence a measure of the brain networks: past and present. *Neuropsychiatric Electrophysiology* 2(1):1.
6. Harris KD, Henze DA, Csicsvari J, Hirase H, & Buzski G (2000) Accuracy of tetrode spike separation as determined by simultaneous intracellular and extracellular measurements. *Journal of neurophysiology* 84(1):401--414.
7. Jung MW, Qin Y, McNaughton BL, & Barnes CA (1998) Firing characteristics of deep layer neurons in prefrontal cortex in rats performing spatial working memory tasks. *Cerebral Cortex* 8(5):437--450.
8. Mitra PP & Pesaran B (1999) Analysis of dynamic brain imaging data. *Biophysical journal* 76(2):691--708.
9. Adhikari A, Topiwala MA, & Gordon JA (2011) Single units in the medial prefrontal cortex with anxiety-related firing patterns are preferentially influenced by ventral hippocampal activity. *Neuron* 71(5):898--910.
10. Abeles M & Gerstein GL (1988) Detecting spatiotemporal firing patterns among simultaneously recorded single neurons. *Journal of neurophysiology* 60(3):909--924.
11. Ndasdy Z, Hirase H, & Czurk (1999) Replay and time compression of recurring spike sequences in the hippocampus. *The Journal of neuroscience : the official journal of the Society for Neuroscience* 19(21):9497--9507.
12. Baeg EH*, et al.* (2003) Dynamics of population code for working memory in the prefrontal cortex. *Neuron* 40(1):177--188.

2. SI Figures

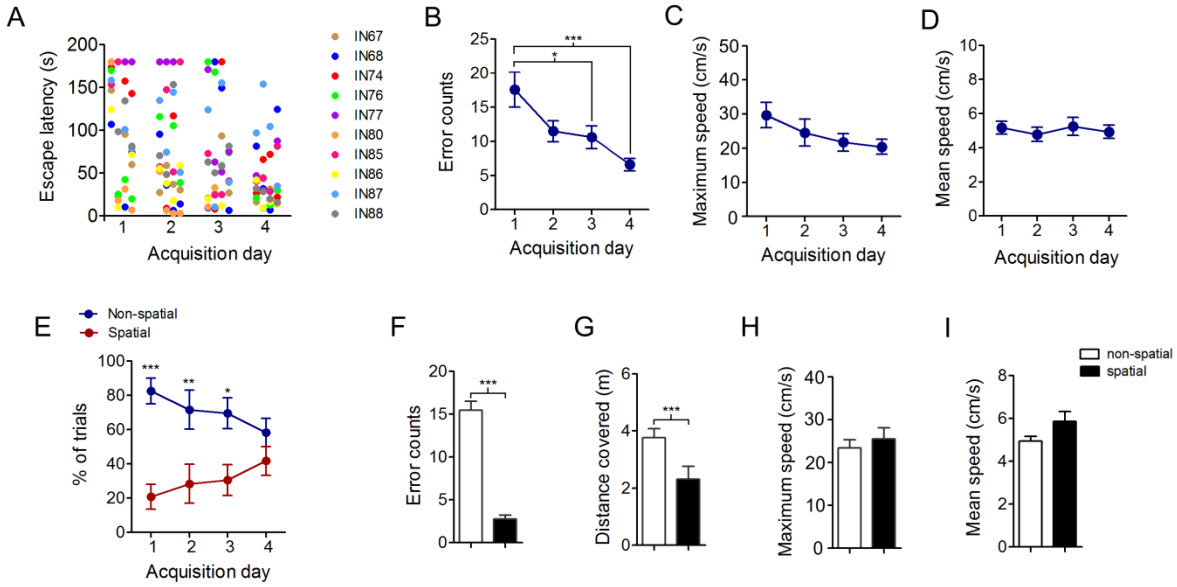

Figure S1. Behavioral performance during task acquisition. (*A*) Escape latency per session during acquisition. Each point represents one session, and each color a different animal. Average error counts (*B*), maximum speed (*C*) and mean speed (*D*) across acquisition days (***, $P < 0.0001$; *, $P < 0.05$, Bonferroni´s multiple comparison test after one-way ANOVA). (*E*) Average percentage of trials in which spatial or non-spatial strategies were implemented across acquisition days. (***, $P < 0.0001$; **, $P < 0.01$; *, $P < 0.05$ Bonferroni´s multiple comparison test after two-way ANOVA). Bar charts of mean error counts (*F*), distance covered (*G*), maximum speed (*H*), and mean speed (*I*) for navigation strategies (***, $P < 0.0001$; t-student test). Data are presented as mean ± SEM.

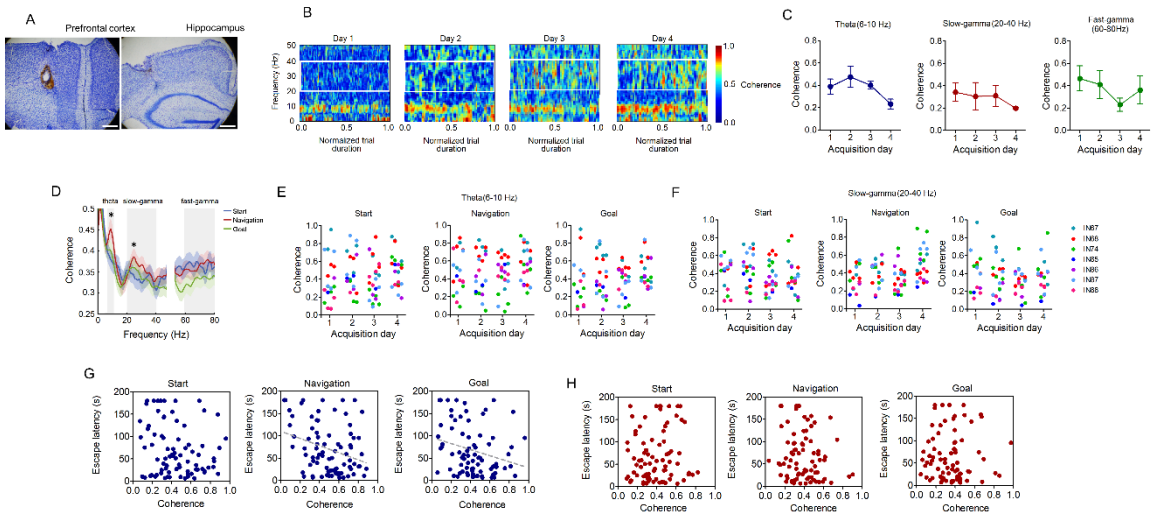

Figure S2. Synchrony between prefrontal cortex and hippocampus during navigation. (*A*) Example coronal sections with electrolytic lesions showing the location of recording sites in the prefrontal cortex (*Left*) and hippocampus (*Right*) (mouse code: IN68). Scale bar: 200 µm. (*B*) Color-coded examples of prefrontal-hippocampus coherograms during the navigation phase of the task at different acquisition days. Color bar indicates the relative magnitude of coherence. Note time scale is normalized to from 0 to 1.0. (*C*) Mean prefrontal-hippocampus coherence during exploration in the home-cage for theta (*Left*), slow-gamma (*Middle*) and fast-gamma (*Right*) oscillations across acquisition days. Data are presented as mean ± SEM, n = 7 animals, 99 trials. (*D*) Mean prefrontal-hippocampus coherence as a function of frequency per task phases. Theta, slow-gamma, and fast-gamma frequency bands are highlighted in gray. Significant differences (signaled by asterisk) were found between start and navigation at theta (frequency peak = 9.8 Hz; $P = 0.037$; Wilcoxon signed rank test) and slow-gamma (frequency peak = 23.5 Hz; $P = 0.022$; Wilcoxon signed-rank test) frequency bands, and between navigation and goal phase at theta (frequency peak = 9.8 Hz; $P = 0.001$; Wilcoxon signed-rank test) and slow-gamma (frequency peak = 23.5 Hz; $P = 0.014$; Wilcoxon signed rank test) frequency bands. (*E*) Prefrontal-hippocampus coherence of theta oscillations per every trial session during start (*Left*), navigation (*Middle*) and goal (*Right*) phases of the task. Each color represents a different animal, as indicated in the legend. (*F*) Same as (*E*), but for slow-gamma oscillations. Note consistent increase in coherence during navigation across sessions and animals. (*G*) Scatter plots of prefrontal-hippocampus coherence for theta oscillations and escape latency for start (*Left*), navigation (*Middle*) and goal (*Right*) phase of the task (Start: $P = 0.161$; r = -0.157; Navigation: $P = 0.024$; r = -0.248; Goal: $P = 0.012$; r = -0.284; Spearman correlation analysis). (*H*) Same as (*G*), but for slow-gamma oscillation (Start: $P = 0.520$; r = 0.072; Navigation: $P = 0.166$; r = -0.155; Goal: $P = 0.646$; r = -0.053; Spearman correlation analysis). See also Table S3.

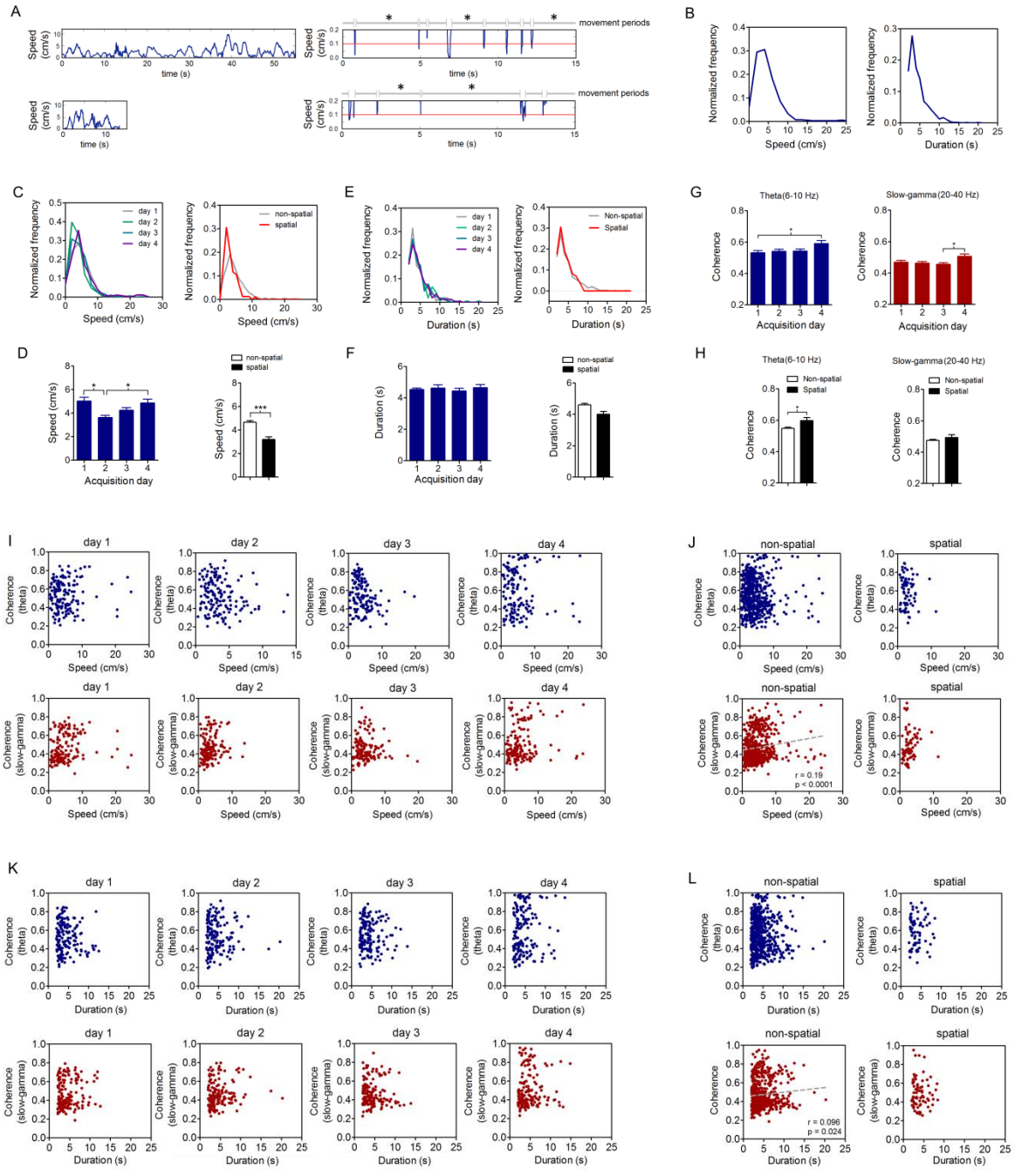

Figure S3. Locomotor activity during navigation. (*A*) Running speed during navigation. *Left*: instantaneous running speed as a function of time throughout the navigation phase of the task for a non-spatial (*Upper*) and a spatial (*Lower*) navigation strategy example. *Right*: zoomed in periods (note scales) from (*A*) to show individual movement periods (*, periods with speed > 0.1 cm/s and duration > 2 s). These movement periods were the unit used for the analysis of locomotor activity. (*B*) Distribution of average speed (*Left*) and duration (*Right*) of all identified movement periods during navigation (n = 614). (*C*) Distributions of

speed for movement periods across acquisition days (*Left*) and navigation strategies (*Right*). (*D*) Bar chart of average speed of movement periods across acquisition days (*Left*) and navigation strategies (*Right*; *, $P < 0.05$; Bonferroni´s multiple comparison test after one-way ANOVA). Data are presented as mean ± SEM. (*E*) Distributions of duration for movement periods across acquisition days (*Left*) and navigation strategies (*Right*). (*F*) Bar chart of average duration of identified movement periods across acquisition days (*Left*) and navigation strategies (*Right*). Data are presented as mean ± SEM. (G) Bar chart of average prefrontal-hippocampus coherence during identified movement periods across acquisition days for theta (*Left*) and slow-gamma (*Right*) frequency bands (*, $P < 0.05$; Bonferroni´s multiple comparison test after one-way ANOVA). Data are presented as mean ± SEM. (*H*) Same as (*G*), but for navigation strategies (***, $P < 0.05$; Bonferroni´s multiple comparison test after one-way ANOVA). Data are presented as mean ± SEM. (*I*) Scatter plots of speed during movement periods vs prefrontal-hippocampus coherence in theta (*Upper*) or slow-gamma (*Lower*) frequency bands across acquisition days. Note during day 4 the emergence of movement periods with high spectral coherence (> 0.8) that were not related to speed. Every point represents an individual movement period (day 1, n = 154; day 2; n = 157; day 3, n = 141; day 4, n = 147; non-spatial, n = 541; spatial, n = 73). (*J*) Same as (*I*), but for navigation strategies. Note weak, significant correlation between slow-gamma coherence and speed for the non-spatial strategy. (*K*) Scatter plots of duration of movement periods vs prefrontal-hippocampus coherence in theta (*Upper*) or slow-gamma (*Lower*) frequency bands across acquisition days. Note during day 4 the emergence of movement periods with high spectral coherence (> 0.8) that were not related to speed. (*L*) Same as (*K*), but for navigation strategies. Note weak, significant correlation between slow-gamma coherence and duration of movement periods for the non-spatial strategy.

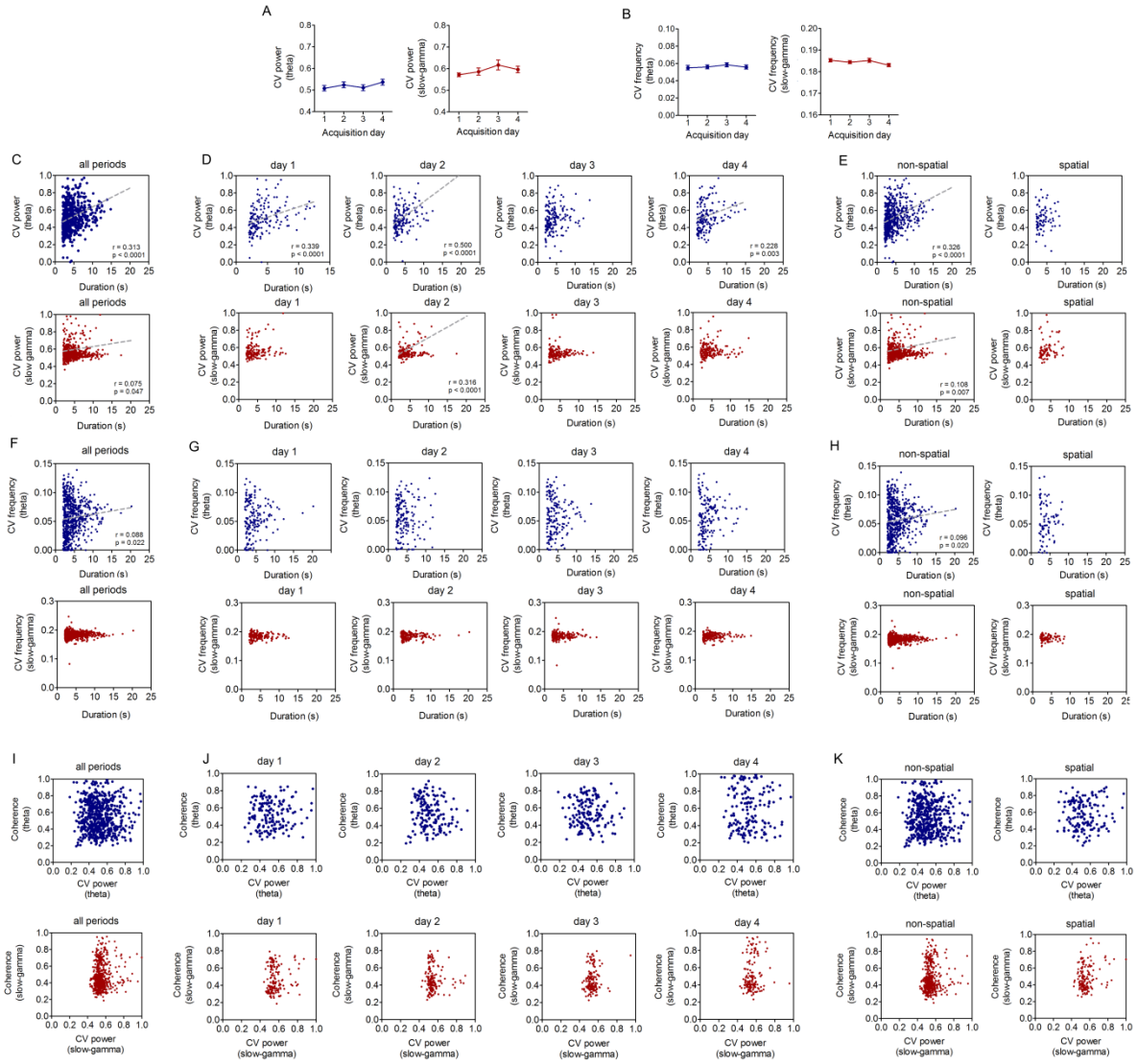

Figure S4. Variability of power and frequency of theta and slow-gamma oscillations. (*A*) Average coefficient of variation of power for theta (*Left*) and slow-gamma (*Right*) oscillations across acquisition days (theta: $P = 0.402$; slow-gamma: $P = 0.272$; one-way ANOVA). Data are presented as mean ± SEM. (*B*) Average coefficient of variation of frequency for theta (*Left*) and slow-gamma (*Right*) oscillations across acquisition days. (theta: $P = 0.790$; slow-gamma: $P = 0.154$; one-way ANOVA). Data are presented as mean ± SEM. (*C*) Scatter plots of coefficient of variation of power vs duration for theta (*Upper*) or slow-gamma (*Lower*) frequency bands of individual movement periods ($n = 657$). Note increased variability as duration of movement periods increase. Lines depict significant regressions obtained from Spearman correlation analysis. (*D*) Scatter plots of coefficient of variation of power vs duration of individual movement periods for theta (*Upper*) or slow-gamma (*Lower*) frequency bands across acquisition days. Every point represents an individual movement period (day 1, n = 164; day 2, n = 166; day 3, n = 165; day 4, n = 162).

Note increased variability as duration of movement periods increase. (*E*) Same as (*D*); but for navigation strategies. Non-spatial, n = 576; spatial, n = 81. Note increased variability as duration of movement periods increase for the non-spatial strategy. *(F*) Scatter plots of coefficient of variation of frequency vs duration for theta (*Upper*) or slow-gamma (*Lower*) frequency bands of individual movement periods (*n* = 657). Note increased variability as duration of movement periods increase. (*G*) Scatter plots of coefficient of variation of frequency vs duration of individual movement periods for theta (*Upper*) or slow-gamma (*Lower*) frequency bands across acquisition days. (*H*) Same as (*G*); but for navigation strategies. *(I*) Scatter plots of coefficient of variation of power vs coherence during individual movement periods for theta (*Upper*) or slow-gamma (*Lower*) frequency bands of individual movement periods. (*J*) Scatter plots of coefficient of variation of power vs coherence during individual movement periods for theta (*Upper*) or slow-gamma (*Lower*) frequency bands across acquisition days. (*K*) Same as (*J*); but for navigation strategies. Note that cortical coherence and variability of cortical oscillations are unrelated.

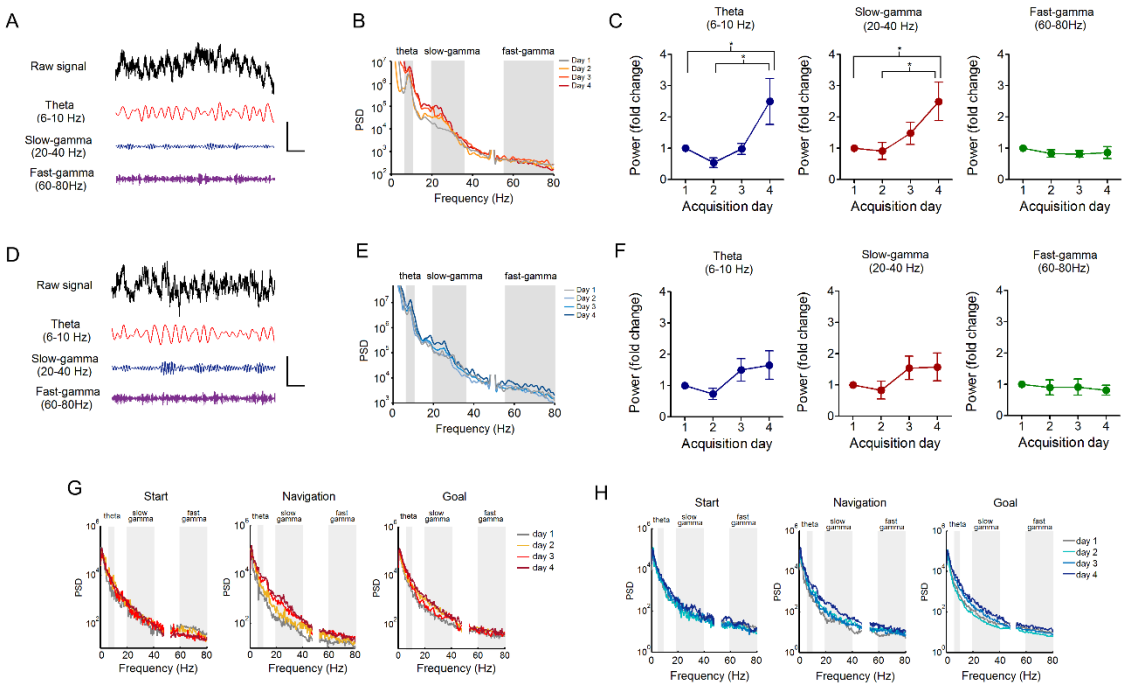

Figure S5. Power spectral density in prefrontal cortex and hippocampus during acquisition of reference spatial memory. Example LFP recordings from prefrontal cortex (*A*) and hippocampus (*D*) during navigation, and filtered for theta (6-10 Hz), slow-gamma (20-40 Hz), and fast-gamma (60-80 Hz) frequency bands. Scale bar for prefrontal cortex: 250 ms; 400 uV; for hippocampus: 250 ms, 500 uV. Power spectra from prefrontal cortex (*B*) and hippocampus (*E*) averaged for acquisition days. Theta, slow-gamma, and fast-gamma frequency bands are highlighted in gray (n = 7 animals, 159 trials). Mean changes in theta (*Left*), slow-gamma (*Middle*), and fast-gamma (*Right*) power relative to the day 1 for prefrontal cortex (*C*) and hippocampus (*F*) (*, $P < 0.05$; Bonferroni´s multiple comparison test after one-way ANOVA). Data are presented as mean ± SEM. (*G*) Averaged power spectra from prefrontal cortex during start (*Left*), navigation (*Middle*), and goal (*Right*) phases across acquisition days. (*H*) Same as (*G*), but for hippocampus. See also Tables S4 and S5.

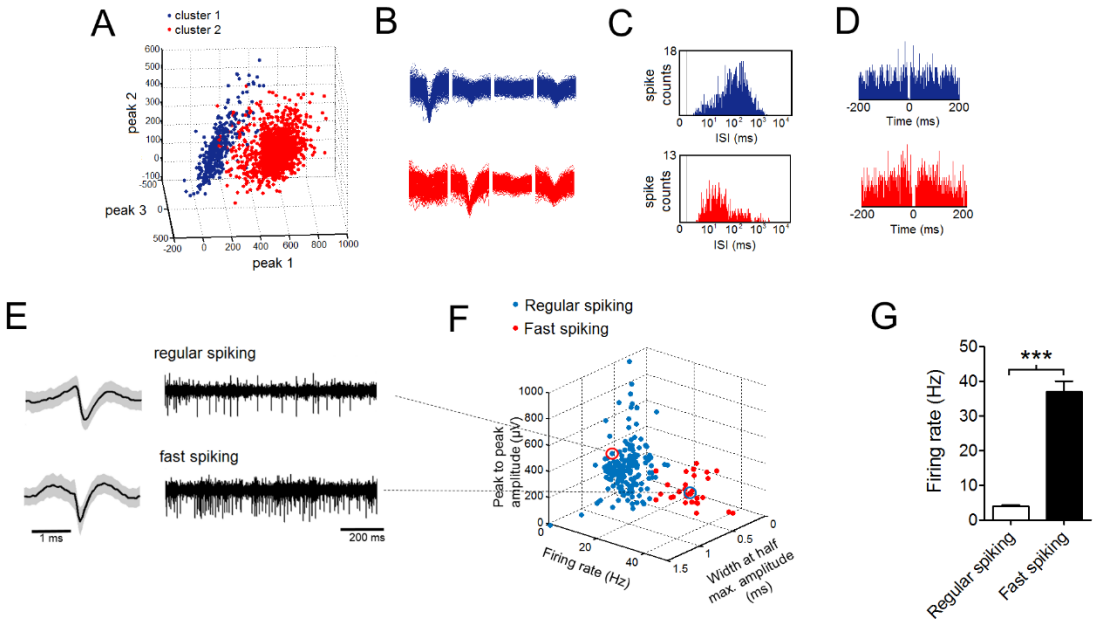

Figure S6. Spike sorting. (*A*) Example cluster plot of the three-dimensional projection for the spike components of two units recorded simultaneously from the same tetrode. Clusters with distinct colors correspond to two different units. (*B*) Superimposed spike waveforms on all four channels from the same tetrode for the clusters of units showed in (*A*). (*C* and *D*) Interspike-interval histograms (*C*) and autocorrelograms (*D*) for clustered units. Colors correspond to clusters in (*A*). (*E*) Example average waveforms and filtered LFP recording (high-pass: 500 Hz) for a regular (unit ID: IN68_41_21) and fast spiking (unit ID: IN76_34_11) single unit. (*F*) Raster plot of the three-dimensional projection of extracellular spikes features: firing rate, peak to peak spike amplitude (measured as the absolute difference between the spike minimum voltage and the maximum positive depolarization), and width at half maximum duration (measured as full width at half maximum amplitude) for all recorded units, in which each point represents one unit. Example units from panel (*E*) are depicted. Spike amplitude was not a resolutive feature for cell-type clustering, however we maintain it for illustration purposes as individual points can be better distinguished. (*G*) Bar chart of mean firing rate for clustered regular and fast spiking units (***, $P < 0.0001$, Mann-Whitney U-test). Data are presented as mean ± SEM.

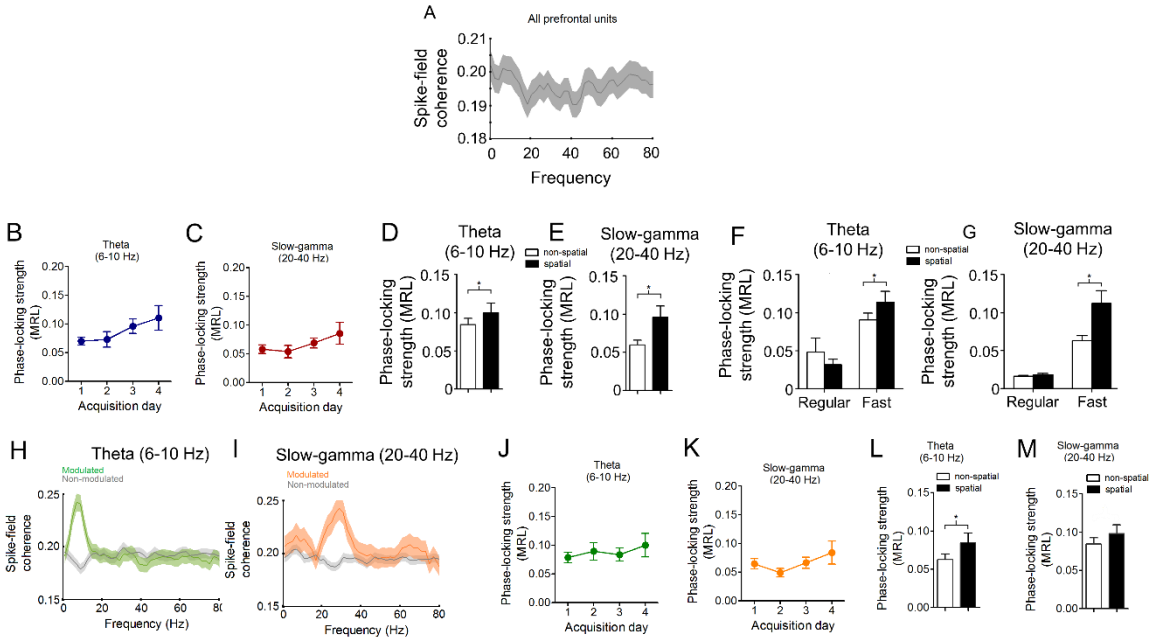

Figure S7. Spike-field coherence and phase locking of prefrontal units to cortical oscillations during task acquisition. (*A*) Average spike-field coherence as function of prefrontal LFP frequency for all recorded prefrontal units. Shading areas depicts SEM. (*B* and *C*) Mean phase locking strength (MRL) of prefrontal units to prefrontal theta (*B*) and slow-gamma (*C*) oscillations across acquisition days. Data are presented as mean ± SEM. (*D* and *E*) Bar charts of phase-locking strength (MRL) of prefrontal units to local theta (*D*) and slow-gamma oscillations (*E*) during the entire behavioral session across navigation strategies (*: $P < 0.05$; Mann-Whitney U-test). Data are presented as mean ± SEM. (*F* and *G*) Bar chart of phase-locking strength (MRL) of prefrontal units to local theta (*F*) or slow-gamma oscillations (*G*) during the navigation phase sorted by cell type (*: $P < 0.05$; Mann-Whitney U-test). (*H* and *I*) Average spike-field coherence as function of LFP frequency of significantly modulated prefrontal units ($P < 0.05$, green or orange) and non-modulated prefrontal units (grey) by hippocampal theta (*H*) and slow-gamma (*I*) oscillations. Shading indicates SEM. (*J* and *K*) Mean phase-locking strength (MRL) of prefrontal units to hippocampal theta (*J*) and slow-gamma (*K*) oscillations across acquisition days. Data are presented as mean ± SEM. (*L* and *M*) Mean phase-locking strength of prefrontal units to hippocampal theta (*L*) and slow-gamma (*M*) band for navigation strategies (*, $P < 0.05$; Mann-Whitney U test). Data are presented as mean ± SEM.

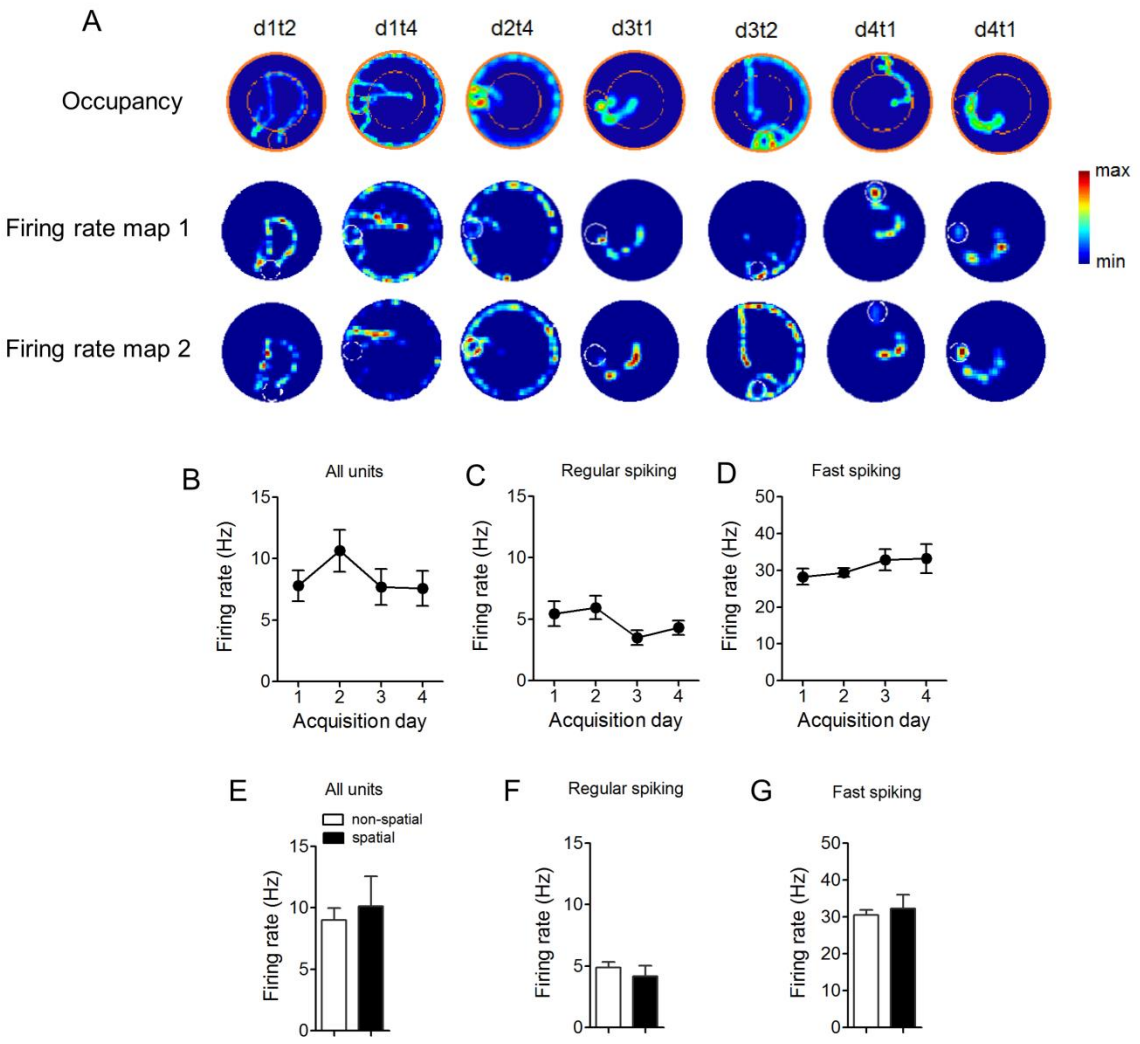

Figure S8. Spatial firing rate maps of prefrontal units. (*A*) Examples of occupation maps during different trials in the Barnes maze (*Upper panels*). Spatial firing-rate maps from two different units simultaneously recorded in the same trials as above (*Lower panels)*. All spatial firing rate maps derive from different units. Day and trial in which occupation and firing-rate maps were acquired is indicated (d: day number; t: trial number). Color bar indicates the magnitude of occupancy or firing rate for each map. Average firing rates for all units (*B*), regular spiking units (*C*), and fast spiking units (*D*) across acquisition days. Data are presented as mean ± SEM. (*E-G*) Same as (*B-D*), but comparing firing rates between navigation strategies. Data are presented as mean ± SEM.

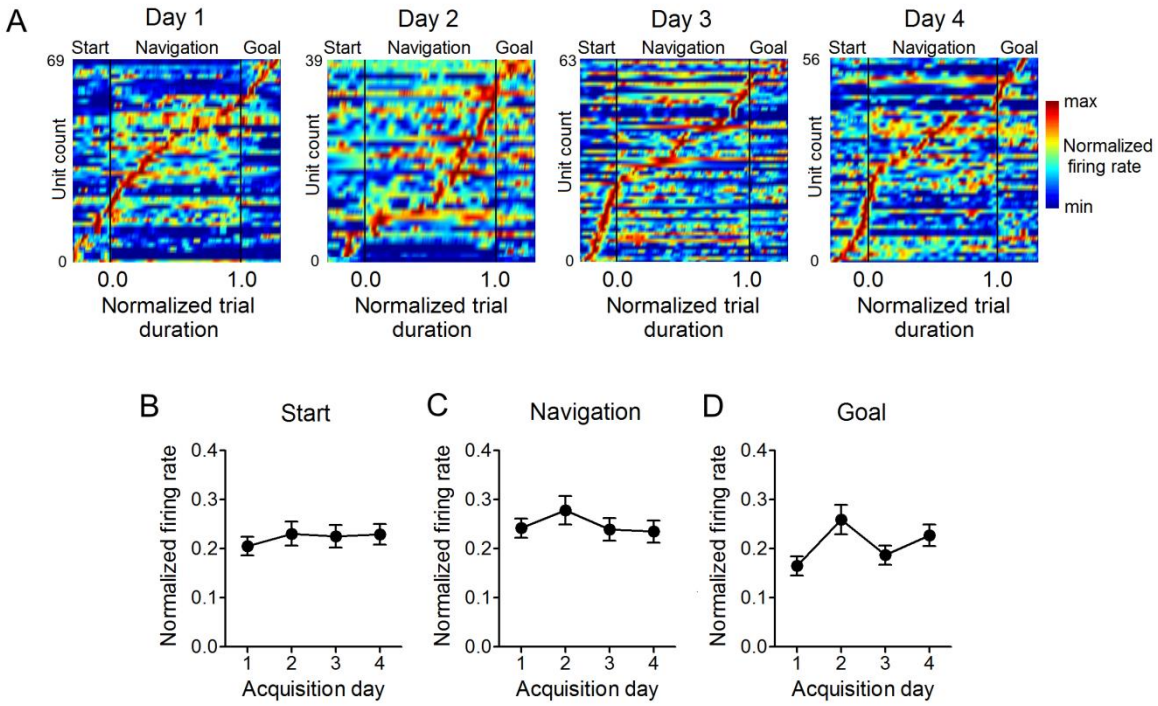

Figure S9. Firing patterns of prefrontal units across acquisition days. (*A*) Normalized firing patterns of individual prefrontal units grouped by acquisition day and sorted by peak firing time. Mean normalized firing rate of spike trains from prefrontal cortex across acquisition days for start (*B*), navigation (*C*), and goal (*D*) phases of the task. Start and goal phases have a fixed duration of 1 minute. The navigation phase varied between 7 and 180 seconds (median = 57.4 seconds). Data are presented as mean ± SEM.

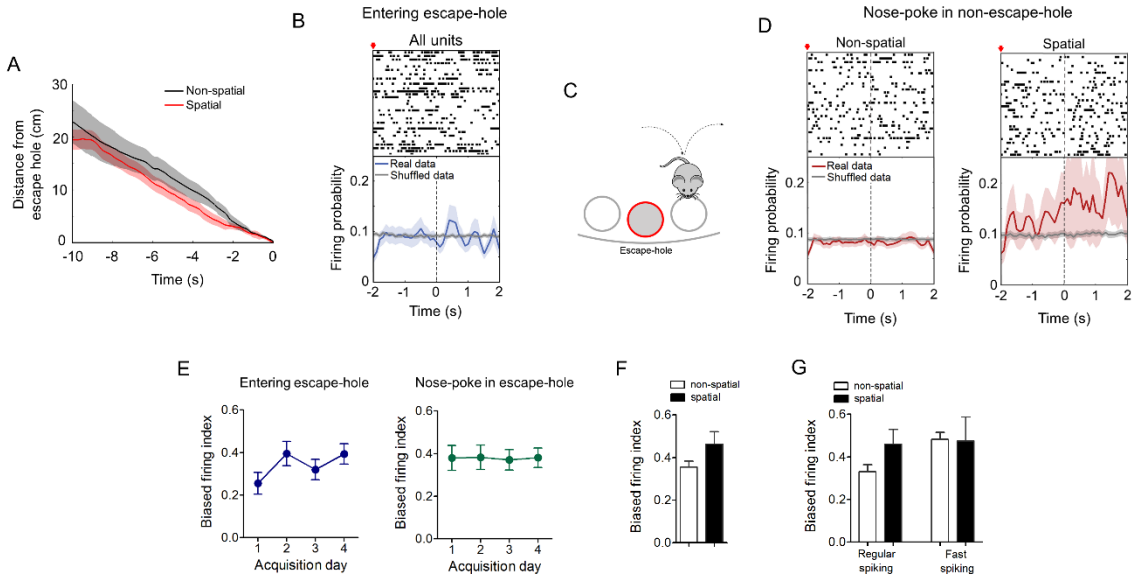

Figure S10. Spatial firing selectivity of prefrontal neurons. We first evaluated the relative position and time intervals of animals with respect to the goal as they approach the escape. To this aim, we focused on the animal's position during the last 10 seconds preceding entrance to the escape hole in order to include trials with spatial strategy, in which case the entire navigation period could last for as little as 10 seconds. We found that the approach speed to the goal was similar for the spatial and non-spatial strategy, as the distance to the escape hole decreased monotonically over time in both conditions during the last 10 seconds before reaching the escape. Given that this locomotor pattern was consistently similar for both strategies during the entire 10 sec-window ($p > 0.05$, Wilcoxson signed rank test); that is, positions and time intervals were preserved, any given time interval could be potentially analyzed. In addition, we noted that 2 seconds before entering into the escape hole, animals were on average at 4 cm from the goal. At that distance, animals were closer to the goal than to any other hole in the maze, suggesting that at this point, the animal's trajectory was directed to the escape hole. Thus, we looked into that time window with more detail. For this, we studied neural activity in the prefrontal cortex during those 2 seconds before reaching the goal. (*A*) Average distance from the escape hole as a function of time preceding reaching the hole for non-spatial and spatial navigation strategies. Shading areas depicts SEM. (*B*) Example raster plots and average normalized peri-event time histograms (PETHs) of all prefrontal units aligned at the time when the mouse enters the escape-hole. Shuffled data are also displayed (gray line). Superior red arrow indicates time at which mice were at 4 cm from the escape hole. Shuffled data are displayed (gray line). Shading areas indicate SEM. (*C*) Schematic diagram of nose-poking in non-escape-holes. (*D*) Example raster plots and average normalized PETHs of the population of prefrontal units recorded during non-spatial (*Left*) or spatial (*Right*) navigation strategies, and aligned at the time of nose-poke of non-escape holes (i.e.; errors). Shuffled data are displayed (gray line).

Shading areas depict SEM. Superior red arrow indicates time at which mice were at 4 cm from the escape hole. (*E*) Average mean biased firing index across acquisition days relative to entering (Left) or nose-poking (Right) on the escape-hole for all prefrontal units (n = 227 units). Data are presented as mean ± SEM. (*F*) Bar charts of the mean biased firing index between strategies during nose-poke in the escape-hole. Data are presented as mean ± SEM. Data are presented as mean ± SEM. (G) Same as (F), but sorted for regular and fast spiking units. Data are presented as mean ± SEM.

3. SI Tables

	Acquisition day				
	1	**2**	**3**	**4**	**total**
Total units	69	40	62	56	**227**
Regular-spiking units	62	32	53	47	**194**
	(89.8 %)	(80.0%)	(85.4%)	(83.9%)	**(85.4%)**
Average firing rate (Hz)	5.4 ± 1.0	5.8 ± 1.0	6.3 ± 1.1	6.8 ± 1.2	
Fast-spiking units	7	8	9	9	**33**
	(10.1%)	(20.0%)	(14.5%)	(16.0%)	**(14.5%)**
Average firing rate (Hz)	28.3 ± 2.1	29.4 ± 1.1	32.8 ± 2.8	33.2 ± 3.9	

Table S1. Summary of single units recorded per day.

Animal ID	**IN67**	**IN68**	**IN74**	**IN76**	**IN77**	**IN80**	**IN85**	**IN86**	**IN87**	**IN88**	
Trials: Failure	1	1	2	2	8	0	3	1	4	2	**24**
Trials: Random	0	2	3	1	3	1	0	0	0	0	**10**
Trials: Serial	11	7	7	9	5	1	7	11	8	10	**76**
Trials: Direct	4	6	3	4	0	8	4	3	4	3	**39**
Total: trials	16	16	15	16	16	10	14	15	16	15	**149**
Trials: Non-spatial strategy	12	10	12	12	16	2	10	12	12	12	**110**
Trials: Spatial strategy	4	6	3	4	0	8	4	3	4	3	**39**
Trials: prefrontal LFP	14	16	14	15	16	8	13	16	16	16	**144**
Trials: hippocampal LFP	14	16	0	0	0	8	13	16	16	16	**99**
Trials: spectral coherence	14	16	0	0	0	8	13	16	16	16	**99**
Regular spiking units	18	88	21	2	19	0	28	0	0	18	**194**
Fast spiking units	0	13	0	16	3	0	1	0	0	0	**33**
Units non-spatial	15	73	18	14	22	0	21	0	0	17	**180**
Units spatial	3	28	3	4	0	0	8	0	0	1	**47**
Units total	18	101	21	18	22	0	29	0	0	18	**227**

Table S2. Summary of navigation strategies per animal.

Source	Sum Sq.	d.f.	Mean Sq.	F	Prob > F
frequency	0.6172	1	0.61717	16.47	0.0001
time	0.6684	3	0.22282	5.95	0.0006
phase	0.3508	2	0.17542	4.68	0.0097
frequency*time	0.0931	3	0.03104	0.83	0.4788
frequency*phase	0.1353	2	0.06763	1.8	0.1657
time*phase	0.1827	6	0.03044	0.81	0.5607
Error	17.4646	466	0.03748		
Total	19.4355	483			

Table S3. Multifactorial ANOVA for variables (oscillatory frequency, gamma or theta; acquisition day, 1-4; and task phase, start, navigation, or goal) modulating cortical coherence.

Source	Sum Sq.	d.f.	Mean Sq.	F	Prob > F
frequency	41.83	2	20.9169	1.82	0.164
time	67.31	3	22.4362	1.95	0.1215
phase	101.52	2	50.7575	4.42	0.0129
frequency*time	51.26	6	8.5436	0.74	0.6152
frequency*phase	24.25	4	6.0614	0.53	0.7158
time*phase	79.81	6	13.3014	1.16	0.3295
Error	3207.1	279	11.495		
Total	3606.02	302			

Table S4. Multifactorial ANOVA for variables (oscillatory frequency, gamma or theta; acquisition day, 1-4; and task phase, start, navigation, or goal) modulating hippocampus LFP spectral power.

Source	Sum Sq.	d.f.	Mean Sq.	F	Prob > F
frequency	2704.2	2	1352.11	1.25	0.2884
time	18599.2	3	6199.74	5.72	0.0008
phase	9933.7	2	4966.86	4.58	0.0108
frequency*time	8565.3	6	1427.56	1.32	0.2484
frequency*phase	4592.6	4	1148.14	1.06	0.3764
time*phase	20269.5	6	3378.26	3.12	0.0055
Error	383602.6	354	1083.62		
Total	39541432.5	746			

Table S5. Multifactorial ANOVA for variables (oscillatory frequency, gamma or theta; acquisition day, 1-4; and task phase, start, navigation, or goal) modulating prefrontal cortex LFP spectral power.

Figure	Test	Condition	Statistic	P
1B	one way ANOVA	Escape latency days	$F_{(3, 147)} = 7.63$	<0.0001
1C	one-way ANOVA	Time in quadrant	$F_{(3, 31)} = 4.773$	0.0082
1E	t-student	Escape latency strategies	$t_{(144)} = 7.48$	<0.0001
2C	one-way ANOVA	Coher theta days	$F_{(3, 81)} = 1.03$	0.381
2D	one-way ANOVA	Coher slow gamma days	$F_{(3, 82)} = 5.06$	0.002
2E	one-way ANOVA	Coher fast gamma days	$F_{(3, 108)} = 0.81$	0.488
3B	Rayleigh	theta	ln(Z) = 4.31	<0.0001
		slow gamma	ln(Z) = 2.34	<0.0001
3E	Mann-Whitney U	MRL theta strategies	U = 3177	0.013
3G	Mann-Whitney U	MRL start strategies	U = 850	0.189
		MRL navigation strategies	U = 1056	0.012
		MRL goal strategies	U = 1584	0.258
3I	Mann-Whitney U	MRL regular spiking strategies	U = 2081	0.0036
	Mann-Whitney U	MRL fast spiking strategies	U = 85	0.542
3K	Spearman correlation	MRL v/s escape latency	r = -0.39	<0.0001
3F	Mann-Whitney U	MRL slow gamma strategies	U = 3166	0.010
3H	Mann-Whitney U	MRL start strategies	U = 996	0.783
		MRL navigation strategies	U =1184	0.0006
		MRL goal strategies	U = 2116	0.279
3J	Mann-Whitney U	MRL regular spiking strategies	U = 1935	0.0006

		MRL fast spiking strategies	U = 80	0.5
3L	Spearman correlation	MRL v/s escape latency	r = -0.43	<0.0001
4C	Mann-Whitney U	Norm rate start strategies	U = 3553	0.655
		Norm rate navigation strategies	U = 2941	0.036
		Norm rate goal strategies	U = 3473	0.501
4D	Mann-Whitney U	Norm rate regular spiking strat	U = 2078	0.045
		Norm rate fast spiking strategies	U = 71	0.354
4E	Spearman correlation	Norm rate v/s escape latency	r = -0.165	<0.001
5B	Wilcoxon signed-rank	Firing probability escape strat		
5D	Wilcoxon signed-rank	Firing probability nose-poke strat		
5E	Mann-Whitney U	Biased all strategies	U = 1708	0.0031
5F	Mann-Whitney U	Biased regular strategies	U = 1010	0.001
		Biased fast stretegies	U = 76	0.714
5G	Spearman correlation	Biased v/s escape latency	r = -0.175	0.004
S1B	one-way ANOVA	Errors days	$F_{(4, 141)} = 3.46$	<0.0003
S1C	one-way ANOVA	Max speed days	$F_{(3, 143)} =$ 0.037	0.197
S1E	two-way ANOVA	% of trials	$F_{(3,68)} = 37.82$	<0.001
S1F	t-student	Error strategies	$t_{(139)} = 8.01$	<0.0001
S1G	t-student	Distance strategies	$t_{(144)} = 7.48$	<0.0001

S1H	t-student	Max speed strategies	$t_{(150)} = 0.62$	0.53
S2C	one-way ANOVA	Coher home theta days	$F_{(3, 16)} = 2.10$	0.149
		Coher home slow gamma	$F_{(3, 16)} = 0.56$	0.650
		Coher home fast gamma	$F_{(3, 16)} = 0.84$	0.492
S2F	one-way ANOVA	Coher slow gamma start	$F_{(3, 16)} = 4.902$	0.179
		Coher slow gamma nav	$F_{(3, 16)} = 11.16$	0.009
		Coher slow gamma goal	$F_{(3, 16)} = 1.295$	0.730
S2I	t-student	Coher theta strategies	$t_{(107)} = 0.17$	0.862
		Coher slow gamma strat	$t_{(107)} = 1.18$	0.240
		Coher fast gamma strat	$t_{(107)} = 2.023$	0.096
S5C	one-way ANOVA	Power theta days PFC	$F_{(3, 35)} = 4.86$	0.0067
		Power slow gamma days PFC	$F_{(3, 35)} = 3.82$	0.019
		Power fast gamma days PFC	$F_{(3, 35)} = 0.581$	0.631
S5F	one-way ANOVA	Power theta days HPC	$F_{(3, 24)} = 2.472$	0.089
		Power slow gamma days HPC	$F_{(3, 23)} = 1.555$	0.231
		Power fast gamma days HPC	$F_{(3, 24)} = 0.184$	0.905
S6G	Mann-Whitney U	Firing rate regular v/s fast	U = 0.001	< 0.0001
S7B	Kruskal-Wallis	MRL theta days	$H_{(3)} = 2.57$	0.461
		MRL slow gamma days	$H_{(3)} = 3.09$	0.377
S7F	Kruskal-Wallis	MRL theta days	$H_{(3)} = 0.453$	0.929
S7I	Mann-Whitney U	MRL theta strategies	U = 2592	0.0057

S7G	Kruskal-Wallis	MRL slow gamma days	$H_{(3)} = 3.096$	0.377
S7H	Mann-Whitney U	MRL slow gamma strategies	U = 2880	0.051
S8B	Kruskal-Wallis	Firing rate all days	$H_{(3)} = 4.046$	0.256
S8C		Firing rate regular days	$H_{(3)} = 5.046$	0.167
S8D		Firing rate fast days	$H_{(3)} = 2.222$	0.527
S8E	Mann-Whitney U	Firing rate all strategies	U = 3966	0.547
S8F		Firing rate regular strategies	U = 2623	0.223
S8G		Firing rate fast strategies	U = 77	0.883
S9B	Kruskal-Wallis	Normalized FR start	$H_{(3)} = 1.347$	0.718
S9C		Normalized FR navigation	$H_{(3)} = 1.457$	0.692
S9D		Normalized FR goal	$H_{(3)} = 8.314$	0.043
S10B	Wilcoxon signed-rank	Firing probability goal all		
S10D		Firing prob nose-poke strat		
S10E	Kruskal-Wallis	Biased index escape days	$H_{(3)} = 4.284$	0.232
		Biased index nose-poke days	$H_{(3)} = 0.019$	0.999
S10F	Mann-Whitney U	Biased index nose-poke strat	U = 1884	0.086
S10G		Biased index nose-poke regular	U = 1170	0.076
		Biased index nose-poke fast	U = 82	0.941

Table S6. Summary of statistical tests.

4. SI Videos

Direct.wmw – chronically implanted mouse navigating the Barnes maze and implementing the direct strategy to find the escape hole.

Random.wmw – chronically implanted mouse navigating the Barnes maze and implementing the non-direct strategy to find the escape hole. In this case, the mouse randomly explores different holes in the maze until finding the escape hole.

Serial.wmw – chronically implanted mouse navigating the Barnes maze and implementing the non-direct strategy to find the escape hole. In this case, the mouse systematically explores neighboring holes until finding the escape hole.